

Chemistry–A European Journal

Supporting Information

Synergistic Biophysical Techniques Reveal Structural Mechanisms of Engineered Cationic Antimicrobial Peptides in Lipid Model Membranes

Frank Heinrich,^[a, b] Aria Salyapongse,^[a] Akari Kumagai,^[a] Fernando G. Dupuy,^[a, c]
Karpur Shukla,^[a, d] Anja Penk,^[e] Daniel Huster,^[e] Robert K. Ernst,^[f] Anna Pavlova,^[g]
James C. Gumbart,^[g] Berthony Deslouches,^[h] Y. Peter Di,^[h] and Stephanie Tristram-Nagle^{*[a]}

Supporting Information
©Wiley-VCH 2019
69451 Weinheim, Germany

Abstract: In the quest for new antibiotics, two novel engineered Cationic Antimicrobial Peptides (eCAPs) have been rationally designed. WLBU2 and D8 (all 8 valines are the D-enantiomer) efficiently kill both Gram-negative and –positive bacteria, but WLBU2 is toxic and D8 non-toxic to eukaryotic cells. We explore protein secondary structure, location of peptides in six lipid model membranes, changes in membrane structure and pore evidence. We suggest that protein secondary structure is not a critical determinant of bactericidal activity, but that membrane thinning and dual location of WLBU2 and D8 in the membrane headgroup and hydrocarbon region may be important. While neither peptide thins the Gram-negative lipopolysaccharide outer membrane model, both locate deep into its hydrocarbon region where they are primed for self-promoted uptake into the periplasm. The partially α -helical secondary structure of WLBU2 in a red blood cell (RBC) membrane model containing 50% cholesterol, could play a role in destabilizing this RBC membrane model causing pore formation that is not observed with the D8 random coil, which correlates with RBC hemolysis caused by WLBU2 but not by D8.

DOI: 10.1002/anie.2016XXXXX

SUPPORTING INFORMATION

Table of Contents

Experimental Procedures (page 3-7)

Including Figure S1 to Fig. S3

Results (page 7-19)

Including Figure S4 to S14

Including Table S1 to S17

SI Acknowledgments (page 19)

References (page 20)

SUPPORTING INFORMATION

Experimental Procedures

Materials for five methods. Synthetic lipids were purchased from Avanti Polar Lipids (Alabaster, AL) except LPS was purified from *P. aeruginosa* (PAO1) and cholesterol was from Nu-Chek-Prep (Waterville, MN). Organic solvents were HPLC grade from Sigma-Aldrich (St. Louis, MO). PBS buffer was from Sigma-Aldrich or Merck/Calbiochem (Darmstadt, Germany). Unlabeled peptides were synthesized by Genscript (Piscataway, NJ). ^{13}C -labeled peptides were synthesized by the Core Unit Peptide Technologies of Leipzig University.

X-ray diffuse scattering (XDS).

XDS general description. Model membranes were prepared using the Rock and Roll procedure¹ which mixes lipids and peptides in organic solvent, plates them onto chromic acid-cleaned silicon wafers and then dries them under vacuum for at least two hours. Lipid:peptide molar ratios varied from 1000:1 to 50:1. Samples were fully hydrated in a thick-walled hydration chamber with mylar windows for x-rays². Full hydration is defined as no further uptake of water, measured by no further increase in lamellar D-spacing. The final D-spacing is the same as a sample submerged under water. X-ray diffuse scattering data were collected at the Cornell High Energy Synchrotron Source (CHESS), Ithaca, NY on three trips using x-ray wavelengths $\sim 1.1 \text{ \AA}$, and at the home source using a Rigaku (Tokyo, Japan) RUH3R rotating anode generator with x-ray wavelength $\sim 1.5 \text{ \AA}$. All samples were measured at 37°C except KDO2 which was measured at 55°C . The XDS data are analyzed using liquid crystal theory with methods described in detail in the SI to Ref. ³. Full hydration causes the membrane stacks to fluctuate, producing lobes of diffuse data⁴⁻⁵, which provide the intensity data that is the basis for the form factors. Taking the Fourier transform of the form factors using a modeling approach⁶ yields the electron density profile which gives structural quantities^{3,7-9}.

XDS materials. The 24-mer peptides WLBU2 and D8 (chemical structures shown in Fig. S1) were synthesized by Genscript (Piscataway, NJ). Purity was $\sim 98\%$ as shown by mass spectroscopy analysis. While their amino acid sequences are identical, all of the valines in D8 are the D-enantiomer. The synthetic lyophilized lipids 1-palmitoyl-2-oleoyl-*sn*-glycero-3-phosphoethanolamine (POPE), 1-palmitoyl-2-oleoyl-*sn*-glycero-3-phospho-(10-*rac*-glycerol) sodium salt (POPG), 10,30-bis-[1,2-dioleoyl-*sn*-glycero-3-phospho]-*sn*-glycerol sodium salt (TOCL, i.e., cardiolipin), 1-palmitoyl-2-oleoyl-*sn*-glycero-3-phosphocholine (POPC), 1,2-dioleoyl-3-trimethylammoniumpropane chloride salt (DOTAP), 1,2-dilauryl-*sn*-glycero-3-phosphocholine (DLPG) and Di[3-deoxy-D-manno-octulosonyl]-lipid A (ammonium salt) (KDO2, 6-chain) were purchased from Avanti Polar Lipids (Alabaster, AL) and used as received. Lipopolysaccharide (LPS) was purified from *Pseudomonas aeruginosa* 01. Mass spectroscopy (Fig. S2) and HPLC determined that this LPS was a 2:1 mixture of *m/z* 1446 (5-chain) and *m/z* 1616 (6-chain). Details of the purification and mass spec are published in Experimental Materials of Ref. ¹⁰. Cholesterol was from Nu-Chek-Prep (Waterville, MN). HPLC grade organic solvents were purchased from Sigma-Aldrich (St. Louis, MO).

WLBU2:	RR WVRR VRR WVRR VVR VVRR WVRR
D8:	RR <u>W</u> RR <u>V</u> RR <u>W</u> RR <u>V</u> RR <u>V</u> RR <u>W</u> RR

Figure S1. Primary structures of WLBU2 and D8. The underlined valines in D8 indicate D-Val substitutions. The net charge of both peptides is +13.

XDS methods. Lipid model membranes were prepared by first dissolving lyophilized lipids in chloroform or KDO2 in trifluoroethanol (TFE)/H₂O (4:1, v/v). These lipid stock solutions were combined to create lipid mixtures in molar ratios mimicking bacterial membranes: Gram-negative inner membrane G(-)(IM), POPE/POPG/TOCL (7 : 2 : 1 molar ratio), Gram-positive membrane, G(+) POPG/DOTAP/POPE/TOCL (6 : 1.5 : 1.5 : 1); eukaryotic membrane POPC/POPE/cholesterol (5 : 1 : 1.8) (23 mol% cholesterol, Euk23), and red blood cell (RBC) eukaryotic membrane (5 : 1 : 6) (50 mol% cholesterol, Euk50). For the outer membrane (OM) of G(-) bacteria, KDO2 rough mutant was used, which contains two octulosonic acid residues in addition to the two mannose residues of Lipid A. A second OM model of LPS/DLPG 1:9 molar ratio was used instead of pure LPS because LPS alone did not undergo thermal fluctuations when fully hydrated. Composition of the bacterial membrane models was based on Ref. ¹¹ and the eukaryotic models were based on Ref. ¹². WLBU2 and D8 stock solutions were prepared by mixing lyophilized powder in hexafluoroisopropanol (HIP). Multilamellar stacked samples for X-ray scattering were prepared by mixing 4 mg of the lipid mixtures plus WLBU2 or D8 into glass test tubes in molar ratios: 1000:1, 500:1, 200:1, 100:1, 75:1 and 50:1 lipid/peptide. When calculating the molecular weight of the peptides, 13 trifluoroacetate counter-ions were included for each peptide for a total gram-molecular weight of 4882. Solvents were removed by evaporation under vacuum and samples were redissolved in appropriate HPLC-grade solvents for spreading (v/v ratios): G(-) IM, HIP/chloroform (2 : 1); G(+), HIP/chloroform (1 : 1); LPS/DLPG TFE/H₂O (10:1); KDO2, chloroform/methanol/H₂O (90:10:1), eukaryotic with 23 mol% cholesterol TFE/chloroform (1 : 1); and eukaryotic with 50 mol% cholesterol, chloroform. These mixtures were plated onto silicon wafers (1 x 15 x 30 mm³) via the Rock-and-Roll method¹ to produce stacks of ~ 1800 well-aligned bilayers, where the silicon wafer is rocked continuously during solvent evaporation. Plating occurred in the fume hood instead of the usual glove box due to the toxicity of HIP. Once immobile, the thin film was additionally evacuated for at least 2 h. The sample was trimmed to a central 5 mm wide strip parallel to the long-edge of the wafer¹. Hydration occurred through the vapor in a thick-walled X-ray hydration chamber².

SUPPORTING INFORMATION

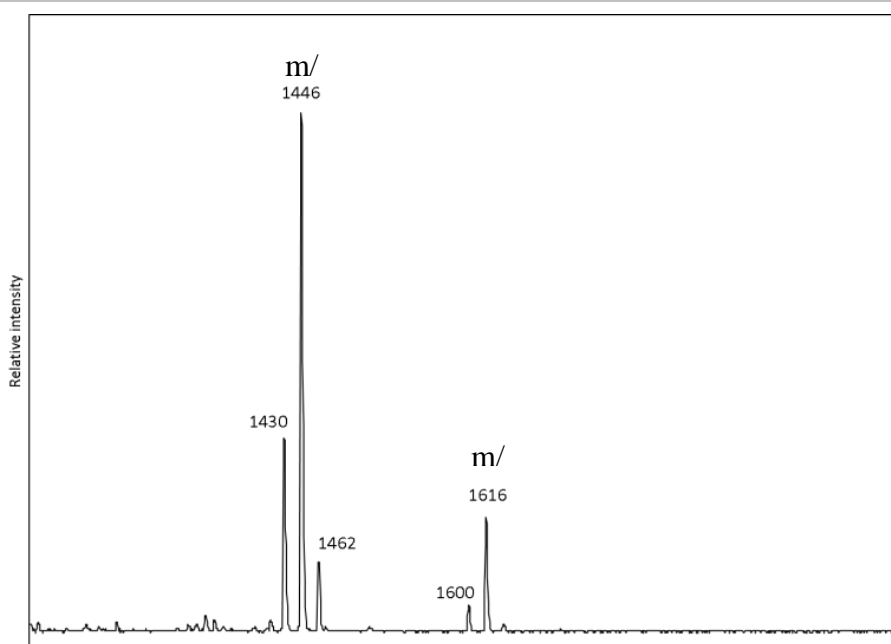


Figure S2. Mass spectrometry of *Pseudomonas aeruginosa* PAO-1 from LPS extracted and converted to lipid A in the lab of Robert K. Ernst.

XDS data collection. Low-angle X-ray diffuse data (LAXS) of fully hydrated, oriented samples were collected at the G1 line at the Cornell High Energy Synchrotron Source (CHESS), Ithaca, NY, on three separate trips using X-ray wavelengths ~ 1.1 Å. Sample-to-detector distances were 387-417 mm. In addition, a laboratory X-ray source RUH3R rotating anode X-ray generator (Rigaku, Tokyo, Japan) with a FOX 2D Focusing Collimator (Xenocs, Sassenage, France) and a Mercury CCD detector (Rigaku) were used with X-ray wavelength 1.5418 Å and S-distance of 280 mm. Full hydration is judged by no further increase in lamellar D-spacing over time. Measurements were carried out in the fluid phase typically at 37°C, except for KDO2 samples, which were studied at 55°C due to the high melting temperature of the lipid.

XDS data analysis. The data analysis of LAXS diffuse data from oriented, fully hydrated samples has been described in several publications^{2-5,10,13} and in great detail in the SI to Ref.³. Backgrounds were first subtracted to remove extraneous air and mylar scattering and the images were laterally symmetrized to increase the signal-to-noise ratio. As the sample nears full hydration, membrane fluctuations occur which produce "lobes" of diffuse X-ray scattering data. Briefly, liquid crystal theory¹⁴ is used to quantitate the thermal fluctuations which yield K_C (bending modulus) and B (compressibility modulus). This theory quantitates the fall-off in intensity in the lateral, q_r direction, in the yellow fitting box shown in Fig. S3. After the elasticity has been quantitated, these parameters are fixed and the LAXS data are fit one additional time, yielding the fitted intensity over the entire q_z range (red box in Fig. S3). These intensity data are continuous and provide the basis for obtaining the form factors which are the Fourier transform of the electron density of the average bilayer in the stack. Typically 2-5 images were averaged before the next model fitting step.

In the second step, the intensity data obtained above are loaded into the Scattering Density Profile (SDP) program⁶ which takes the square root and carries out the Lorentz and absorption corrections. At this point the data have been transformed into form factors, which are fit by comparing to a model of a bilayer with component groups. Since the SDP program is based on molecular volumes, the resulting electron density profiles are on an absolute scale ($e/\text{Å}^3$). The SDP program yields structural results, such as area/lipid, D_{HH} (peak head-to-head thickness) and $2D_C$ (hydrocarbon thickness). It also yields position of the peptides in the bilayer, although this is more reliably obtained using neutron scattering (see below). Volumes for the control lipids are as in SI in Ref.³.

SUPPORTING INFORMATION

Figure S3. Diffuse LAXS data obtained at CHESS. The yellow fitting box is used to quantitate elasticity by analyzing the lobes of diffuse data that are caused by thermal fluctuations at full hydration. Lobes are identified with yellow numbers. The beam spot is visible through the semi-transparent beam stop (dark rectangle) at the bottom of the 2D CCD image.

Neutron reflectivity (NR).

NR general description. Lipid:peptide mixtures are cosolubilized in organic solvent, dried under vacuum and hydrated via bath sonication. A single membrane bilayer was deposited onto a lipid-tethered gold-covered 3" silicon wafer using the vesicle fusion method¹⁵. NR data were collected at the NGD-MAGIK reflectometer¹⁶ at the NIST Center for Neutron Research (Gaithersburg, MD) over a momentum transfer range 0-0.25 Å⁻¹. 6-hour scans were collected in either H₂O or D₂O at 37°C for all models except KDO2 model, which was collected at 55°C. Data were analyzed at NIST; 1D-structural profiles are parameterized using a continuous distribution model¹⁷ using Refl1D software packages¹⁸.

NR materials. Lipids and peptides were as for x-ray experiments. LPS model consisted of LPS:DLPG 1:3 and KDO2 model consisted of KDO2:DLPG 1:11, while the x-ray experiment used neat KDO2. DLPG was added to both OM membrane models in order to achieve complete bilayer coverage on the tethered silicon wafer.

NR methods. While XDS uses a stack of membranes, NR probes a single bilayer attached to a gold substrate. 3" diameter, 5 mm thick n-type Si:P [100] wafers (EI-Cat Inc., Ridgefield Park, NJ) were cleaned with the SC-1 step of a RCA clean¹⁹. The substrates were coated with Cr (~20 Å) and Au (~150 Å) by magnetron sputtering (ATC Orion; AJA International, Scituate, MA). Coated substrates were soaked in a 7:3 (mol/mol) ethanol solution of HC18²⁰ and β-mercaptoethanol at a total concentration of 0.2 mM to form a self-assembled monolayer (SAM). Substrates were assembled in NCNR fluids cells¹⁸ and 5 mg/mL solutions of vesicles in 2 M NaCl of the desired lipid composition were allowed to incubate the dry SAM for ~2 h. Afterwards, the system was flushed with pure water to complete stBLM formation which is shown in a scheme with the NR results (below).

NR data collection. NR measurements were performed at the CGD-Magik reflectometer¹⁶ at the NIST Center for Neutron Research (NCNR). Reflectivity curves were recorded for momentum transfer values $0.01 \leq q_z \leq 0.25 \text{ \AA}^{-1}$. For each measurement, adequate counting statistics were obtained after 5–7 h. The NCNR fluids cell¹⁸ allows for in situ buffer exchange; therefore, subsequent measurements were performed on the same sample area. The entire flow cell was maintained at room temperature. After in situ completion of the stBLM, NR data were sequentially collected with D₂O and H₂O in the measurement cell. Buffer exchange was accomplished by flushing ~10 ml of buffer through the cell (volume ~1.3 ml) using a syringe. Temperature during the scan was 37°C for all of the lipid models except 55 °C for KDO2 model.

NR data analysis. 1D-structural profiles of the substrate and the lipid bilayer along the lipid bilayer normal were parameterized using a continuous distribution model as described earlier¹⁷. The component volume occupancy (CVO) profile of the protein was defined by a Hermite spline with control points on average 15 Å apart. The spatial extension of the protein along the bilayer normal determined the number of control points which were iteratively refined during model optimization. Optimization of model parameters was performed using the *ga refl* and *Refl1D* software packages developed at the NCNR¹⁸. All reflectivity curves of one data set were fit simultaneously to the same model, sharing fit parameters, for example, for the solid substrate. A Monte Carlo Markov Chain-based global optimizer¹⁸ was used to determine fit parameter confidence limits.

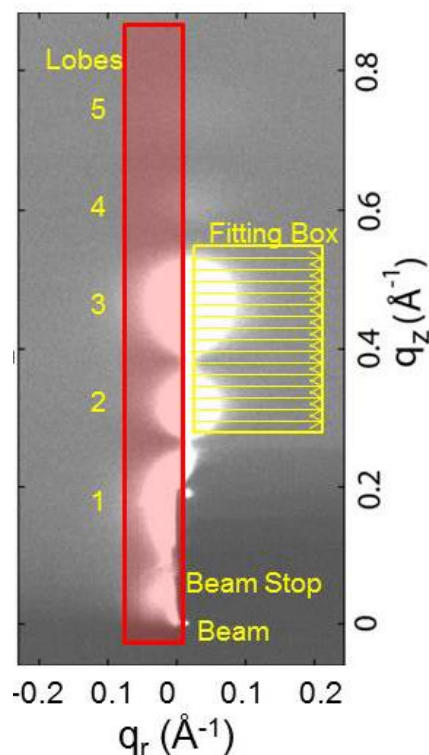
Circular Dichroism (CD).

CD general description. Unilamellar vesicles (ULVs) of ~600 Å diameter were prepared using an Avanti Extruder. Concentrated ULVs were added to 10 μM peptide in 15 mM PBS with pH ~7. Data were collected in 3 mL quartz cuvettes using a Jasco J-715 CD spectrometer at 37°C. OriginPro was used to carry out a linear least squares fit of the smoothed ellipticity traces to four secondary structural motifs representing α-helix, β-sheet, β-turn and random coil²¹. This analysis gives a percentage match of each of the secondary structural motifs to the total sample ellipticity.

CD materials. Dulbecco's phosphate buffered saline (PBS) buffer was purchased from Sigma/Aldrich (St. Louis, MO) and diluted 1:10 with MilliQ water, since 150 mM PBS has significant ellipticity. Peptides and lipids were as for X-ray scattering.

CD methods. Although initial experiments were carried out with oriented thin films, better control over concentration was achieved using unilamellar vesicles (ULVs) prepared by pushing 100 μl of 20 mg/ml lipid in 15mM PBS 31 times through Nucleopore filters of size 500 Å using 0.2 ml Hamilton syringes in an Avanti Extruder. The resulting ULV concentration was initially 20 mg/ml, but due to loss of lipid on the filter, 15 mg/ml as determined gravimetrically. A small amount of stock ULV solution was added to 3 ml of 10 μM WLBU2 to create lipid:peptide molar ratios between 1:1 and 25:1. The samples remained at room temperature for ~16 hours before the CD measurement. The pH was measured with a Radiometer pH 161 pH meter (Copenhagen, Denmark) after the CD experiment.

CD data collection. Data were collected in the Center for Molecular Analysis at Carnegie Mellon. Samples in 3 mL quartz cuvettes with a path length of 1 cm were loaded into a Jasco J-715 CD Spectrometer and allowed to equilibrate for 5 minutes at 37°C. The samples were scanned from 190 to 240 nm 10-20 times and the results were averaged. Temperature was controlled via a Peltier element and water circulation through the



SUPPORTING INFORMATION

sample compartment. Nitrogen gas was used at a flow rate between 20 and 25 cubic feet/hour (CFH). The parameters for scanning were at a speed of 100 nm/min, a step size of 1.0 nm, a response time of 1 second, a bandwidth of 1 nm, and a sensitivity of 20 mdeg. The Jasco J-715 uses Spectra Manager software to provide both ellipticity and absorption results.

CD data analysis. OriginPro was used to analyze the raw ellipticity data from each sample run. Adjacent averaging between 1 and 3 adjacent nm was used to smooth the data. Backgrounds of appropriate lipids were also smoothed using adjacent averaging. After smoothing, the backgrounds were normalized to the same concentration as in the sample. They were then subtracted from the smoothed sample data. Once smoothing and background subtraction were completed, the data were fit to the Brahms-Brahms secondary structural motifs using a least squares fit analysis. The Brahms-Brahms data set is available in Ref. ²¹. This analysis gives a percentage match of each of the secondary structural motifs to the total sample ellipticity.

SUPPORTING INFORMATION

Nuclear Magnetic Resonance (NMR).

NMR general description. Lipids for the G(-) IM or Euk50 model membranes were cosolubilized with WLBU2 or D8 in organic solvent in a 30:1 lipid:peptide molar ratio. After solvent removal by lyophilization, 15 mM PBS buffer was added to a 50 wt% concentration. Samples were hydrated by freeze-thaw with centrifugation. Samples were loaded into 4 mm MAS rotors and measured at 37°C. NMR spectra were analyzed by programs written in Mathcad as described in ^{22,23}.

NMR materials. PBS from Merck/Calbiochem was diluted 1:10 at pH 7.4. WLBU2 and D8 labeled with ¹³C and ¹⁵N were synthesized by the Core Unit Peptide Technologies at Leipzig University and their labeling schemes are shown below. In addition to the two peptides shown unlabeled WLBU2 and D8 were also used. Lipids were as for X-ray.

WLBU2: RR WVRR VRR WVRR VVR VVRR WVRR

D8: RR W_vRR vRR W_vRR v_vR v_vRR W_vRR

The ¹³C and ¹⁵N labeled primary structures of WLBU2 and D8. The lowercase underlined valines in D8 indicate D-Val substitutions. The red lettering indicates amino acids with ¹³C and ¹⁵N atoms. The net charge on both peptides is +13. These two peptides were only used for the secondary structure determination. Unlabeled WLBU2 and D8 were used for the remaining NMR experiments.

NMR methods. POPE, POPG, and TOCL were dissolved in chloroform with a molar ratio of 7:2:1 using POPE-*d*₃₇:POPG:TOCL or POPE:POPG-*d*₃₇:TOCL. D8 and WLBU2 were dissolved in methanol and added to the lipid mixture in a 1:30 peptide:lipid molar ratio. The solvents were then removed by evaporation, and lyophilization was performed with the addition of cyclohexane. The lyophilization process was repeated once and the powder was transferred to a small Eppendorf tube to be weighed. The diluted PBS buffer was added to a 50wt% concentration. Then ten cycles of freeze-thaw were performed using liquid nitrogen and a 40°C oven, with 1 minute of centrifuging after each freeze cycle.

For solution NMR samples, peptides were dissolved in 15 mM PBS buffer (including 5% D₂O). Samples with 50% TFE contained the same amount of PBS and D₂O. Peptide concentration was roughly 1.5 mM and all samples contained 60 μM TMSP-*d*₄ for internal chemical shift calibration.

NMR data collection. NMR experiments were carried out using Avance I 750 MHz, Avance Neo 700 MHz, Avance III 600 MHz, and DRX 300 MHz NMR spectrometers at the University of Leipzig. All samples measured at 37°C.

²H and ³¹P NMR static spectra were acquired either on 300 MHz (operating at 46.07 MHz for ²H and 121.49 MHz for ³¹P) or 750 MHz (operating at 114.91 MHz for ²H and 303.03 MHz for ³¹P) NMR spectrometers equipped with probes using a 5 mm solenoid coil. Using a phase-cycled quadrupolar echo sequence, ²H NMR spectra were accumulated with NS = 4k (750 MHz) or 10k (300 MHz) using a spectral width of ± 250 kHz. 90° pulse lengths varied between 3.2 and 3.4 μs, the echo time was 30 μs (750 MHz) or 50 μs (300 MHz) and a relaxation delay of 1 s was used. For the ³¹P NMR spectra, a recycle delay of 2.5 s, Hahn echo times of 60 μs (750 MHz) or 50 μs (300 MHz) and low power proton decoupling (bb) during acquisition were used. The 90° ³¹P pulses varied between 2.8 and 3.0 μs (300 MHz) and 26k scans were accumulated, at the 750 MHz spectrometer the 90° pulse was 5.9 μs and 2k scans were accumulated per spectrum. For ³¹P NMR spectra processing using an exponential line broadening with 50 Hz was applied. Afterwards, NMR spectra were analyzed by programs written in Mathcad as described in ^{22,23}.

¹³C CP and DARR MAS spectra were recorded using an Avance III 600 MHz spectrometer equipped with a 4 mm spinning module operating at 150.9 MHz for ¹³C. For CP NMR spectra, a MAS frequency of 10 kHz, an ¹H excitation pulse of 4 μs, a CP contact time of 700 μs, a ¹H CP spin lock field of ~ 40 kHz, a recycle delay of 2.5 s and a ~62 kHz SPINAL64 decoupling during acquisition were used. 1k scans were accumulated and a 75 Hz exponential line broadening was used for processing. Additionally, for the 2D DARR spectra, a 90° ¹³C pulse length of 4 μs and a DARR mixing time of 100 ms with a ¹H rf-field strength of 10 kHz were used, 128 increments - with 752 transients each - were accumulated. For processing, zero filling in both dimensions (f1: 512 and f2: 1k) was applied, in f1 a squared cosine function (SSB = 2) and in f2 Gaussian function (LB = -100 Hz, GB 0.17) was used. Finally, spectra were analyzed in NMRFAM-SPARKY²⁴.

Solution NMR experiments of peptides in the absence of any membrane mimetics in 10-fold diluted PBS including 5% D₂O were acquired using an Avance Neo 700 MHz NMR spectrometer (operating at 176.05 MHz for ¹³C, 70.95 MHz for ¹⁵N) equipped with an 5 mm inverse triple resonance probe with z-gradients. For the assignment of Cα and Cβ resonances, gradient-enhanced ¹H-¹³C HSQCs as well as 2D ¹H-¹³C HSQC-TOCSYs were recorded with and without 50 vol% Trifluoroethanol (TFE). Each NMR spectrum was acquired with 128 increments and a spectral width of 16 ppm (¹H) and 80 ppm (¹³C), a recycle delay of 1 s and typically 16 scans (HSQC) or 80 scans (HSQC-TOCSY) per increment. Typical 90° pulse lengths were 8.5 μs for ¹H, 12 μs for ¹³C and 35 μs for ¹⁵N (used for refocusing). During acquisition of 3 k data points in the direct dimension a garp decoupling with a field strength of 3.57 kHz was applied on ¹³C. In case of the HSQC-TOCSY (80 ms mixing time with a spin lock field of 10 kHz using DIPSI-2) only 2 k data points were collected due to the additional ¹⁵N decoupling (1.14 kHz). If TFE was present, an additional low power presaturation on the TFE resonance was used during the recycling delay. For processing zero filling in both dimensions (f1: 128 and f2: 4 k for HSQC, 2 k for HSQC-TOCSY) was applied, in f1 a squared sine function (SSB = 4) and in f2 an exponential window function (LB = 2 Hz) was used.

Differential Scanning Calorimetry (DSC).

DSC general description. DPPC:peptide molar ratios between 1000:1 and 50:1 were prepared by co-solubilizing lipid and peptides in organic solvent, which was then removed by overnight evaporation under vacuum. MilliQ water was added for a final concentration of 1.5 mg/ml. Samples were hydrated by temperature cycling through the T_M with vortexing. Specific heat as a function of temperature was measured with the Microcal MC-II (Northampton, MA). Data were analyzed using OriginPro and a Voigt peak fitting analysis. Enthalpy values of individual peaks were calculated by integrating the area of the peaks and normalizing with respect to DPPC ²⁵.

DSC materials. Peptides were as for X-ray. 1,2-Dipalmitoylphosphatidylcholine (DPPC) was purchased from Avanti Polar Lipids (Alabaster, AL) and used as received.

SUPPORTING INFORMATION

DSC methods. 3 mg of DPPC was dissolved in chloroform. WLBU2 was dissolved in HIP and appropriate amounts were added to the DPPC in chloroform to construct molar ratios from 1000:1 to 50:1 lipid/peptide. Solvent was removed by overnight evaporation and 2 ml of MilliQ water was added for a final concentration of 1.5 mg/ml. Samples were hydrated by temperature cycling between 60 and -20 °C, with vortexing at each temperature three times.

DSC data collection. Samples were loaded into the Microcal (Northampton, MA) MC-II sample cell with a glass filling syringe; heated sample volume was 1.202 ml. Data were collected without compressed air. The scan rate was 12.7 °C per hour with a filter constant of 1 second.

DSC data analysis. Once scans were complete the data were loaded into OriginPro where a background scan of water vs. water was subtracted. Then the data were decomposed into two peaks using a Voigt peak fitting analysis with the peak position fixed and a baseline fixed at zero. Enthalpy values were calculated by integrating the area of peak 1 and peak 2 and normalizing with respect to the known enthalpy of DPPC = 8 kcal/mol²⁵.

Molecular Dynamics (MD) Simulation of KDO2.

MD general description. The simulated 72-lipid KDO2 bilayer was built based on previous simulations of an LPS-containing membrane²⁶. After 200-ns of equilibration, the area/KDO2 reached 160.7 +/- 0.8 Å² (averaged over the last 50 ns), in excellent agreement with Fig. 2C in the main text. A monomer of WLBU2 was added initially at a distance of 10 Å from the membrane surface and then simulated for 400 ns, resulting in the interaction shown in Fig. 6A in the main paper. KDO2:WLBU2 molar ratio was 76:1.

MD methods. KDO2 simulations with and without WLBU2 were performed using NAMD 2.13²⁷. The CHARMM36 lipid force field and CHARMM36m protein force field were used for lipids and peptide, respectively^{28,29}. All covalent hydrogen bonds were kept rigid, which allowed for a 2-fs time step. Van der Waals interactions were cut off at 12 Å, with a force-based smoothing function applied between 10 and 12 Å to ensure a smooth decay to zero. The particle mesh Ewald summation method was used for long-range electrostatic interactions³⁰, which were calculated every two time steps. Temperature was kept constant at 328 K using Langevin dynamics. Pressure was maintained at 1 atm using the Langevin piston method³¹, with the pressure in the plane of the membrane held separately from that in the orthogonal direction.

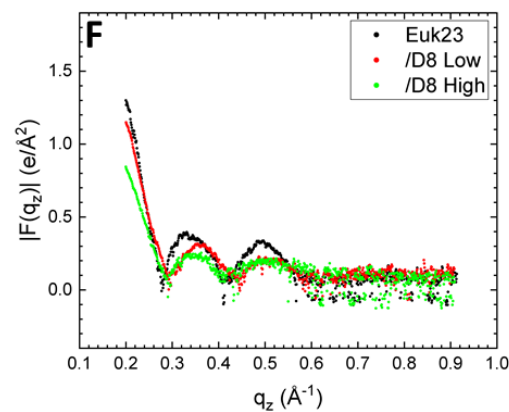
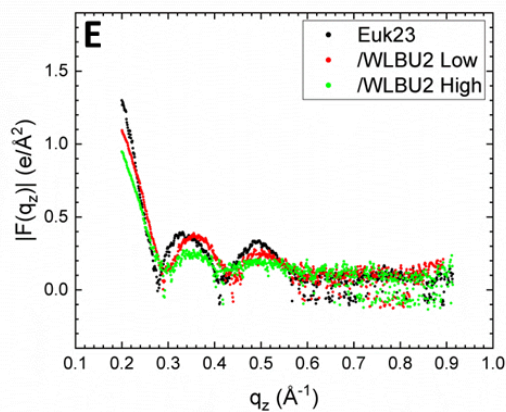
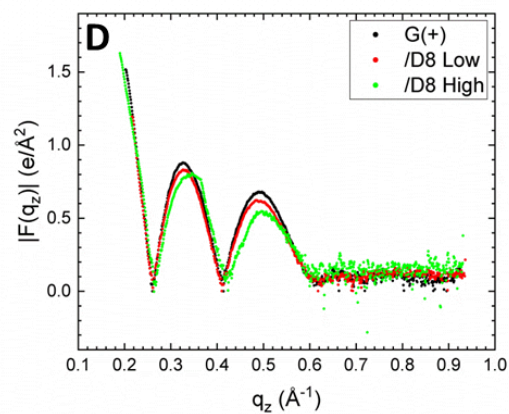
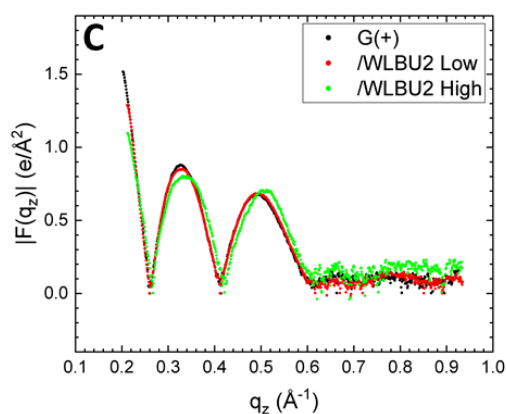
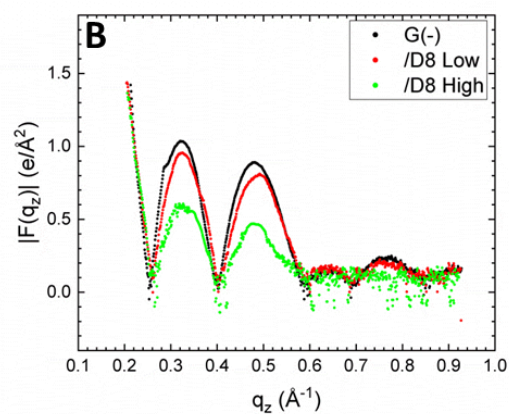
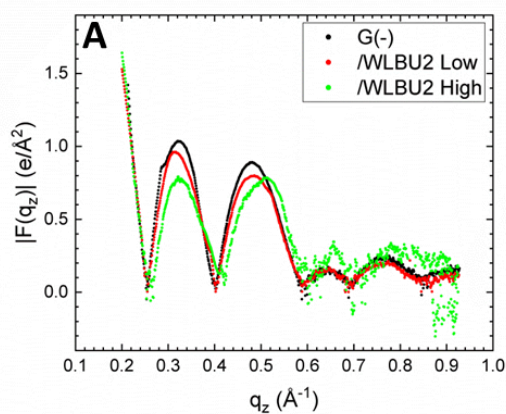
A bilayer containing 72 lipid A molecules (36 per leaflet), each having two attached KDO sugars, was constructed based on previous simulations of an LPS-containing membrane²⁶. The membrane was solvated with TIP3P water³² on both sides and 432 Na⁺ ions were added to neutralize the -6e charge on each KDO2 molecule (-4e on lipid A and -1e on each KDO residue). Over the course of a 200-ns simulation, the area/KDO2 for this membrane equilibrated to 160.7 +/- 0.8 Å² (averaged over the last 50 ns), in excellent agreement with that in Fig. 2C in the main text.

For systems with WLBU2, the peptide was added to the equilibrated membrane system. The peptide was placed oriented horizontally (helical axis in the membrane plane) 10 Å away from the membrane surface, with overlapping water molecules removed. The whole new system was minimized and water and ions were equilibrated for 1 ns while membrane and peptide atoms were restrained using a harmonic force constant of 2 kcal*mol⁻¹*Å⁻¹. Next, all restraints were removed and the system was simulated for an additional 400 ns to observe WLBU2 approach and insert into the headgroup region of the membrane. Simulated form factors and electron-density profiles were produced using the SimtoExp software³³. Code is freely available on the WEB.

Results**X-ray diffuse scattering (XDS).**

SUPPORTING INFORMATION

Form factors for all of the membrane models containing WLBU2 and D8 are shown in Fig. S4. For each membrane model a low (1000:1 or 500:1) and high (100:1 or 75:1) lipid:peptide molar ratio was used since our previous publication, which used several concentrations, showed a stiffening of the G(-) IM and G(+) models at low concentration and a softening of these models at high concentration¹⁰. It was of interest to investigate if these material parameters had structural counterparts (results summary shown in Fig. 2 in the main paper).



SUPPORTING INFORMATION

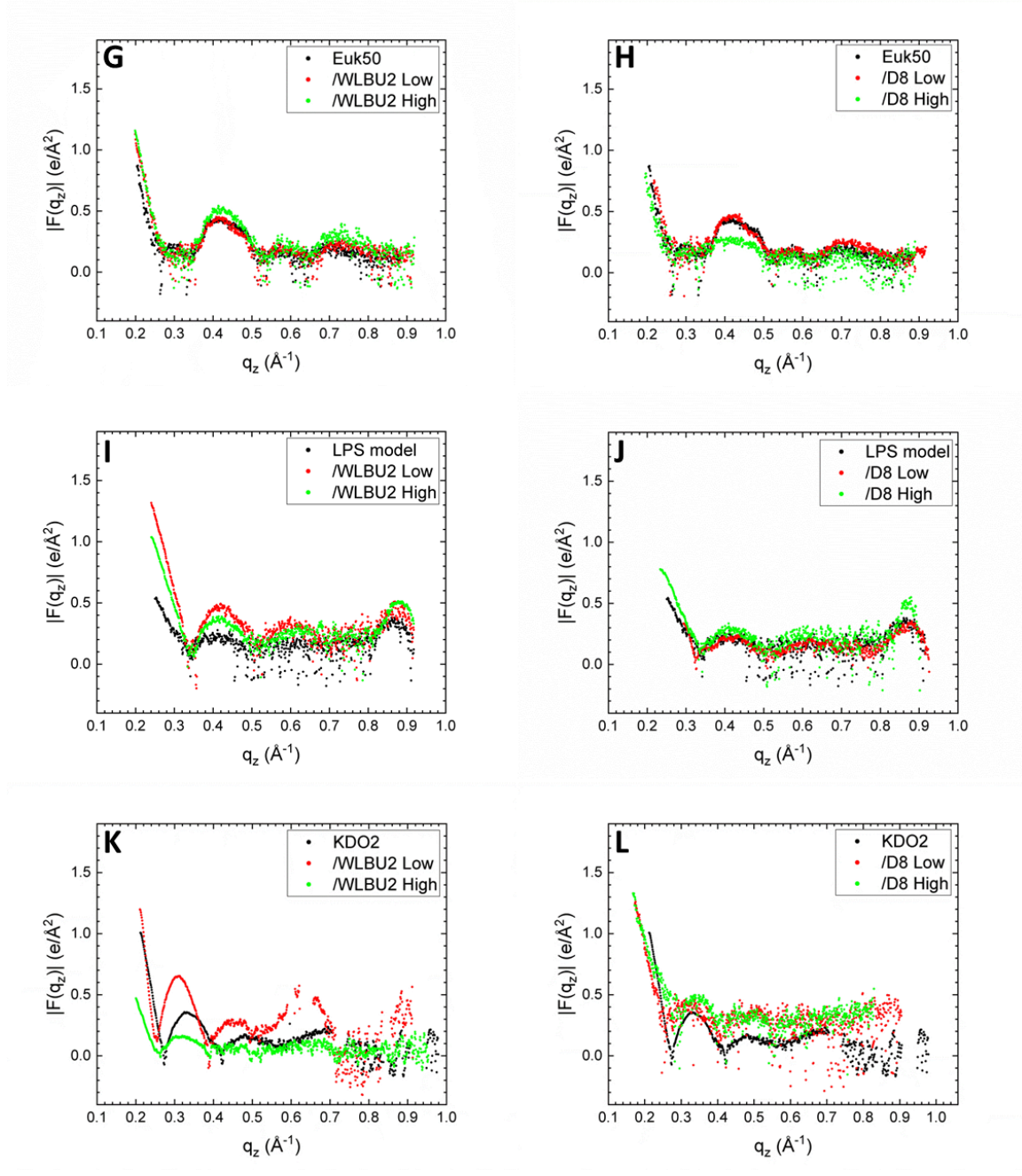


Figure S4. Form factors resulting from the SDP program. (A) G(-)/WLBUE2, (B) G(-)/D8, (C) G(+)/WLBUE2, (D) G(+)/D8, (E) Euk23/WLBUE2, (F) Euk23/D8, (G) Euk50/WLBUE2, (H) Euk50/D8, (I) LPS model (LPS:DLPG 1:9)/WLBUE2, (J) LPS model/D8, (K) KDO2/WLBUE2, (L) KDO2/D8.

SUPPORTING INFORMATION

Neutron reflectivity (NR).

NR probes tethered bilayers such as that shown in Fig. S5. NR yields the position of the peptides in the different membrane models, shown as an envelope in the main paper in Fig. 3 with 68% confidence limits. The Y-axis in Fig. 3 is the component volume occupancy while the X-axis is the distance from the gold substrate in Angstroms. Examples of raw data collected at NIST are shown in Fig. S6. In addition to the component volume occupancy graphs shown in Fig. 3 in the main paper, the NCNR fitting program yields details about the bilayer completeness and peptide position. These results are reported in Tables S1-S6.

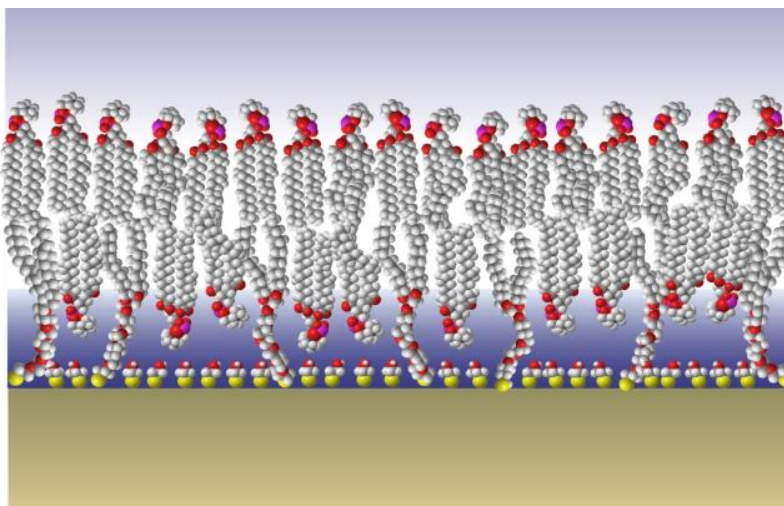


Figure S5. Sparsely tethered bilayer on a gold layer on a silicon wafer. Tethers are lipids with oleic acid in both chains. (Figure reproduced with permission from ¹⁵).

SUPPORTING INFORMATION

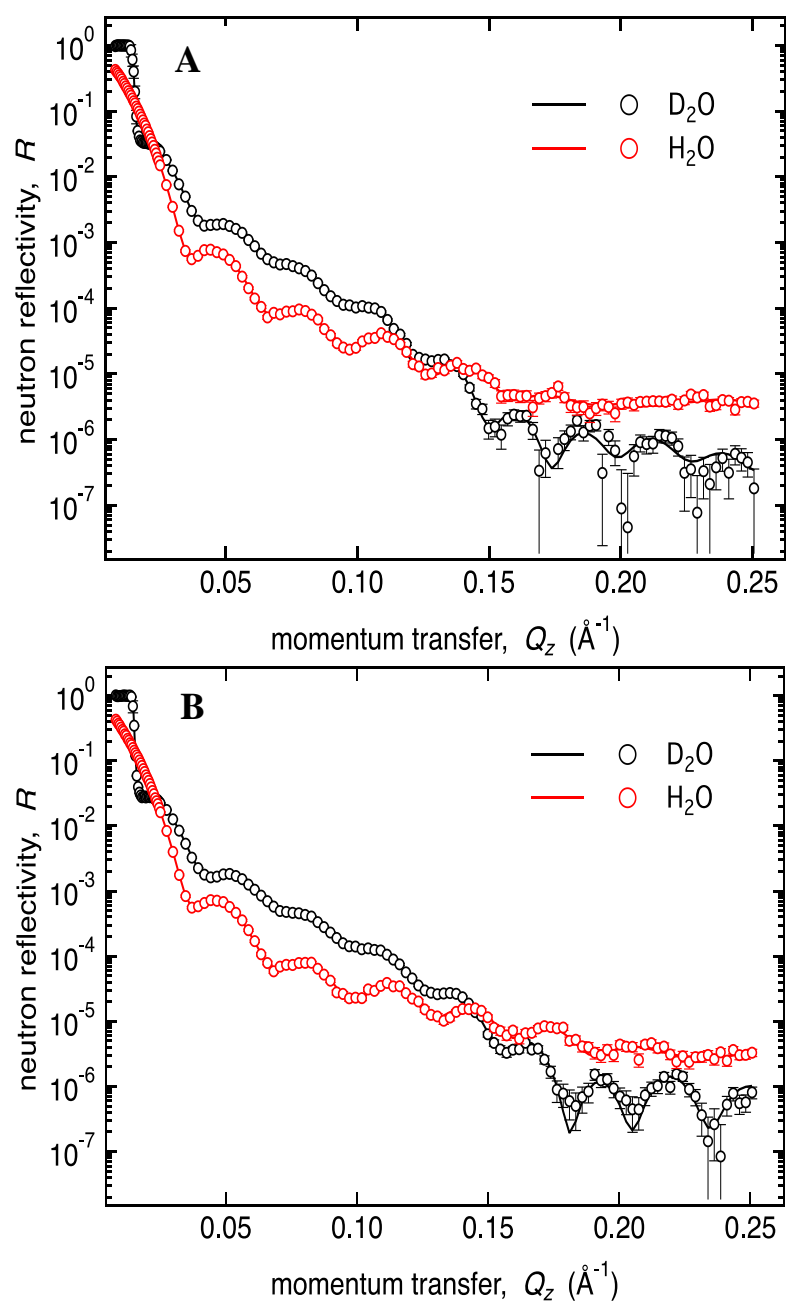


Figure S6. Neutron reflectivity scattering length profile of (A) WLBU2/G(-) and (B) D8/G(-).

SUPPORTING INFORMATION

Table S1. G(-)/peptide NR results

Parameter	/WLBU2	/D8
Hydrocarbon thickness outer lipid leaflet (Å)	10 ± 2	10 ± 3
Bilayer completeness (%)	96 ± 2	100 ± 1
Fraction of protein in hydrocarbons	0.3 ± 0.1	0.4 ± 0.1
Fraction of protein in outer headgroups	0.3 ± 0.1	0.4 ± 0.1
Fraction of protein in bulk solvent	0.26 ± 0.08	0.14 ± 0.05
Peak Position from headgroup / solvent interface (Å)	-3 ± 3	-5 ± 1

As shown in Table S1, the bilayer is nearly 100% complete in G(-) IM models with either WLBU2 or D8, which is a necessary precondition for the results shown in Fig. 3A,B in the main text. For both WLBU2 and D8, the fraction of peptide in the hydrocarbon is nearly equal to the fraction of peptide in the headgroup region, with a smaller fraction of peptide in the bulk solvent. This indicates penetration of both peptides into both the headgroup and hydrocarbon regions of G(-) IM. These results were repeated three times; the results were the same if the peptides were pre-embedded with the lipids, or added from solution to a pre-formed lipid bilayer.

Table S2. G(+)/peptide NR results

Parameter	/WLBU2	/D8
Hydrocarbon thickness outer lipid leaflet (Å)	14 ± 4	9.0 ± 0.5
Bilayer completeness (%)	100 ± 1	100 ± 1
Fraction of protein in hydrocarbons	0.4 ± 0.1	0.6 ± 0.1
Fraction of protein in outer headgroups	0.3 ± 0.1	0.3 ± 0.1
Fraction of protein in bulk solvent	0.24 ± 0.04	0.08 ± 0.05
Peak Position from headgroup / solvent interface (Å)	-12 ± 7	-12 ± 7

As shown in Table S2, the bilayer is ~100% complete in G(+) model with either WLBU2 or D8 which is a necessary precondition for the results shown in Fig. 3C,D in the main text. For both WLBU2 and D8, the fraction of peptide in the hydrocarbon is slightly larger than the fraction of peptide in the headgroup region, with a smaller amount of peptide in the bulk solvent. This indicates penetration of both peptides into both the G(-) IM headgroup and hydrocarbon regions.

Table S3. Euk23 NR results

Parameter	/WLBU2	/D8
Hydrocarbon thickness outer lipid leaflet (Å)	12 ± 2	8 ± 2
Bilayer completeness (%)	100 ± 1	100 ± 1
Fraction of protein in hydrocarbons	0.65 ± 0.1	0.65 ± 0.1
Fraction of protein in outer headgroups	0.3 ± 0.1	0.1 ± 0.02
Fraction of protein in bulk solvent	0.1 ± 0.1	0.25 ± 0.05
Peak Position from headgroup / solvent interface (Å)	-14 ± 3	-19 ± .8

As shown in Table S3, the bilayer is ~100% complete in Euk23 model with either WLBU2 or D8, which is a necessary precondition for the results shown in Fig. 3E,F in the main text. The fraction of peptide in the hydrocarbon is the same for both peptides, but fraction in the headgroup region is slightly larger for WLBU2 than for D8. This indicates penetration of both peptides into both the Euk23 headgroup and hydrocarbon regions.

Table S4. Euk50 NR results

Parameter	/WLBU2	/D8
Hydrocarbon thickness outer lipid leaflet (Å)	12 ± 3	16 ± 1
Bilayer completeness (%)	100 ± 1	90 ± 1
Fraction of protein in hydrocarbons	0.3 ± 0.1	0.1 ± 0.1
Fraction of protein in outer headgroups	0.4 ± 0.1	0.4 ± 0.1
Fraction of protein in bulk solvent	0.3 ± 0.1	0.5 ± 0.1
Peak Position from headgroup / solvent interface (Å)	-3 ± 2	1 ± 4

As shown in Table S4, the bilayer is ~90-100% complete in Euk50 model with either WLBU2 or D8, which is a necessary precondition for the results shown in Fig. 3G,H in the main text. With 50% cholesterol, WLBU2 penetrates into the hydrocarbon to a ~3X greater extent than does D8, while both peptides penetrate equally into the headgroup region. More D8 remains in the bulk solvent than does WLBU2, with the peak position -2 Å for WLBU2 (towards the bilayer) and 1 Å for D8 (towards the solvent) compared to the solvent interface.

SUPPORTING INFORMATION

Table S5. LPS:DLPG (1:3) NR results

Parameter	/WLBUE2	/D8
Hydrocarbon thickness outer lipid leaflet (Å)	7 ± 1	9 ± 3
Bilayer completeness (%)	100 ± 1	99 ± 1
Fraction of protein in hydrocarbons	0.28 ± 0.07	0.5 ± 0.2
Fraction of protein in outer headgroups	0.35 ± 0.07	0.3 ± 0.1
Fraction of protein in bulk solvent	0.32 ± 0.05	0.15 ± 0.09
Peak Position from headgroup / solvent interface (Å)	-3 ± 2	-10 ± 10

As shown in Table S5, the bilayer is ~100% complete in the OM membrane model LPS:DLPG (1:3) with either WLBUE2 or D8, which is a necessary precondition for the results shown in Fig. 3I,J in the main text. In this OM model both peptides penetrate deeply into the hydrocarbon interior, with very little protein remaining in the headgroup. There is little difference between the peptides.

Table S6. KDO2:DLPG (1:11) NR results

Parameter	/WLBUE2	/D8
Hydrocarbon thickness outer lipid leaflet (Å)	7.1 ± 0.5	7 ± 2
Bilayer completeness (%)	85±1	98±2
Fraction of protein in hydrocarbons	0.8±0.1	0.6± 0.2
Fraction of protein in outer headgroups	0.05±0.04	0.1±0.1
Fraction of protein in bulk solvent	0.1±0.1	0.1±0.1
Peak Position from headgroup / solvent interface (Å)	-21±6	-20±10

As shown in Table S6, the bilayer is 85-98% complete in the OM model KDO2:DLPG (1:11) with either WLBUE2 or D8, which is a necessary precondition for Fig.3K,L in the main text. In this OM model both peptides remain primarily in the headgroup region, with D8 penetrating to a slightly greater extent into the hydrocarbon region.

Circular Dichroism (CD).

The CD results of nine different multi-component experiments are summarized below. Effects of WLBUE2 concentration in water, 15 mM PBS buffer, pH, lipid:peptide molar ratio and membrane model were tested.

Table S7. Effect of WLBUE2 concentration in water, pH 7.0, 37°C

Sample	α-helix%	β-sheet%	β-turn%	Random%	R ²
5 μMolar	0	39	0	61	0.99
10 μMolar	0	54	0	46	0.82
13 μMolar	3	35.5	2.5	59	0.99
20 μMolar	3	50.5	1	45.5	0.85
30 μMolar	0	47	0	53	0.82
40 μMolar	4	36	2	59	0.99
Average	1.7±1.7	43.7±7.9	0.9±1.0	53.9±6.9	

As shown in Table S7, WLBUE2 in water is primarily a random coil structure with significant β-sheet, and very little helical content. The ellipticity data collected for the 10 μM sample had the highest amplitude, so this concentration was chosen for subsequent experiments. The R² value indicates the goodness of fit. All of these fits were judged as acceptable.

Table S8. Effect of 15 mM PBS buffer, pH 7.3, 37°C

Sample	PBS	α-helix%	β-sheet%	β-turn%	Random%	R ²
10 μMolar	15mM	4	35	0	57	0.99

As shown in Table S8, 15 mM PBS buffer had almost no effect on secondary structure compared to the average of the samples in water. Subsequent samples were carried out with 15 mM PBS to control the pH.

Table S9. Effect of pH, 37°C

pH	α-helix%	β-sheet%	β-turn%	Random%	R ²
6.4	5	36	1	59	0.96
7.0	5	36	1	58	0.96
7.5	6	34	0	60	0.99

As shown in Table S9, a 10 μM sample of WLBUE2 in 15 mM PBS buffer is unaffected by changing the pH near neutral.

SUPPORTING INFORMATION

Table S10. Effect of G(-)IM ULVs, pH 6.4 – 6.9, 37°C

Sample (molar ratio)	α -helix%	β -sheet%	β -turn%	Random%	R ²
1:1.5 WLBU2/G(-)IM	11	35	0	53	0.98
1:2.3 WLBU2/G(-)IM	14	35	0	51	0.98
1:3 WLBU2/G(-)IM	23	32	0	45	0.96
1:7.5 WLBU2/G(-)IM	62	38	0	0	0.90
1:10 WLBU2/G(-)IM	66	35	0	0	0.95
1:12 WLBU2/G(-)IM	51	24	25	0	0.92
1:15 WLBU2/G(-)IM	70	12	18	0	0.91
1:22.5 WLBU2/G(-)IM	81	9	10	0	0.93

As shown in Table S10, when G(-) IM ULVs are added to 10 μ M WLBU2 the helical content is larger than in pure water or in 15 mM PBS. While the helical content increased with a greater peptide:lipid ratio, aggregation occurred at molar ratios higher than 1:10, so subsequent experiments were carried out with a 1:10 molar ratio.

Table S11. Effect of G(+) membrane model, pH 7.2-7.4, 37°C

Sample (molar ratio)	α -helix%	β -sheet%	β -turn%	Random%	R ²
1:20 WLBU2/G(+)	79	21	0	0	0.94

When WLBU2 was added to G(+) ULVs in 15 mM PBS, there was considerable aggregation causing noisy data, so the sample in Table

S11 was microprobe sonicated. As shown, this sample was primarily α -helical with some β -sheet, similar to the helical content of WLBU2 in G(-) IM ULVs.

Table S12. Effect of LPS Micelles, pH 6.4-6.8, 37°C

Sample (molar ratio)	α -helix%	β -sheet%	β -turn%	Random%	R ²
1:0 WLBU2/LPS	0	54	0	46	0.94
1:1 WLBU2/LPS	4	57	0	40	0.97
1:2 WLBU2/LPS	4	48	0	48	0.92
1:3 WLBU2/LPS	11	51	0	38	0.96
1:4 WLBU2/LPS	11	58	0	33	0.93
1:5 WLBU2/LPS	41	35	0	24	0.85

As shown in Table S12, helical content increased up to ~40% as the LPS concentration increased in 15 mM PBS. When LPS was >1:5 peptide:lipid molar ratio, there appeared a strong, sharp minimum from the LPS background, thus obscuring the

protein motifs, even with proper background subtraction. When LPS was mixed with water, the solution became clear, indicating that a micelle had formed. This occurred in all of the samples in Table S12 indicating that LPS was in micellar form in these experiments, which is ideal for CD spectroscopy, since the background is low.

Table S13. Effect of Eukaryotic models, pH 7.2-7.3, 37 °C

Sample (molar ratio)	α -helix%	β -sheet%	β -turn%	Random%	R ²
1:25 WLBU2/Euk23	14	33	0	53	0.80
1:25 WLBU2/Euk50	23	22	0	55	0.84

As shown in Table S13, the percentage of α -helix was smaller when WLBU2 was mixed with ULVs in 15 mM PBS containing

the Euk23 model or the Euk50 model compared to with G(-) IM or G(+) membrane models. Results are shown for the 1:25 molar ratios with WLBU2, but the 1:10 molar ratio results were similar. When these samples were sonicated the results were similar.

Table S14. Effects of KDO2, pH 7.2-7.3, 55 °C

Sample (molar ratio)	α -helix%	β -sheet%	β -turn%	Random%	R ²
1:16 WLBU2/KDO2	67	27	0	6	0.97

As shown in Table S14, the α -helical content of WLBU2 in KDO2 was similar to that of

WLBU2 in G(-)IM or G(+) models. This sample was microprobe sonicated in 15 mM PBS for a total of two minutes in order to reduce aggregation.

SUPPORTING INFORMATION

Nuclear Magnetic Resonance (NMR).

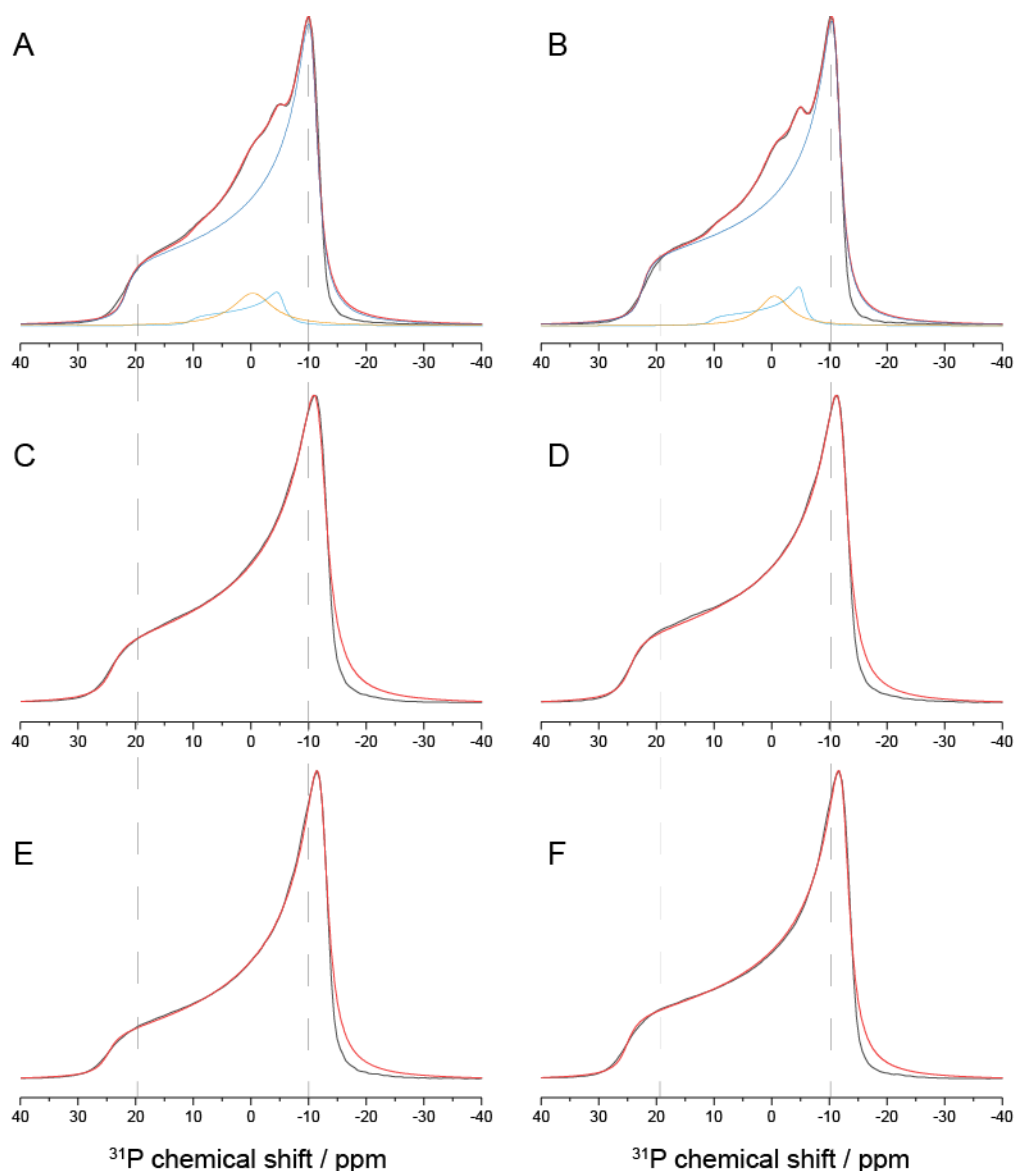


Figure S7. Static ^{31}P NMR spectra of G(-) IM mixture (POPE/POPG/TOCL 7:2:1 molar ratio) shows that all samples are in the lamellar liquid crystalline phase. (A) G(-) IM mixtures with POPG- d_{31} , (B) G(-) IM mixture with POPE- d_{31} , (C) WLB2 + G(-) IM mixture with POPG- d_{31} , (D) WLB2 + G(-) IM mixture with POPE- d_{31} , (E) D8 + G(-) IM mixtures with POPG- d_{31} , (F) D8 + G(-) IM mixture with POPE- d_{31} +D8. Static ^{31}P NMR (red lines), simulated data (black lines). The vertical, dashed lines represent the chemical shift anisotropy ($\Delta\sigma$) of the pure lipids and are used to guide the eye.

For additions of both WLB2 and D8, $\Delta\sigma$ increased, which indicates a reduced amplitude of motion for ^{31}P or altered headgroup orientation compared to pure G(-) IM model. In Fig S7A,B, the spectra consist of a major component with an anisotropy $\Delta\sigma$ of roughly 33ppm (the simulated contribution to experimental red spectrum shown in dark blue). Furthermore, a second minor component with $\Delta\sigma = 15\text{ppm}$ (light blue) and an isotropic peak (orange) were observed. A value $\Delta\sigma \approx 33\text{ppm}$ for POPE and POPG may seem rather unusual, as the normal reported value for POPC is around 47ppm. However, taking into account the G(-) IM mixture, values $\approx 31\text{ppm}$ for TOCL and 34ppm for PE (20°C in a molar ratio of CL:PE:PC 1:2:2)³⁴ and 34ppm for DMPG³⁵ at 40°C have been reported, and therefore our measured values agree well with the literature. For comparison, all simulated anisotropy parameters $\Delta\sigma$ for the major observed component are shown in Table S15.

Table S15. Simulated chemical shift anisotropy $\Delta\sigma$ (ppm) for the major observed component (reflecting both – POPE and POPG – in each measurement) from the static ^{31}P NMR spectra of the different samples. All errors are $\sim \pm 1\text{ppm}$.

SUPPORTING INFORMATION

$\Delta\sigma$ for the major component in ppm in the G(-) IM mixture

Sample	POPG- d_{31}	POPE- d_{31}	Average
Pure G(-) IM lipids	32.4	33.6	33.0
G(-) IM +WLBU2	36.2	36.8	36.5
G(-) IM +D8	37.2	37.7	37.5

SUPPORTING INFORMATION

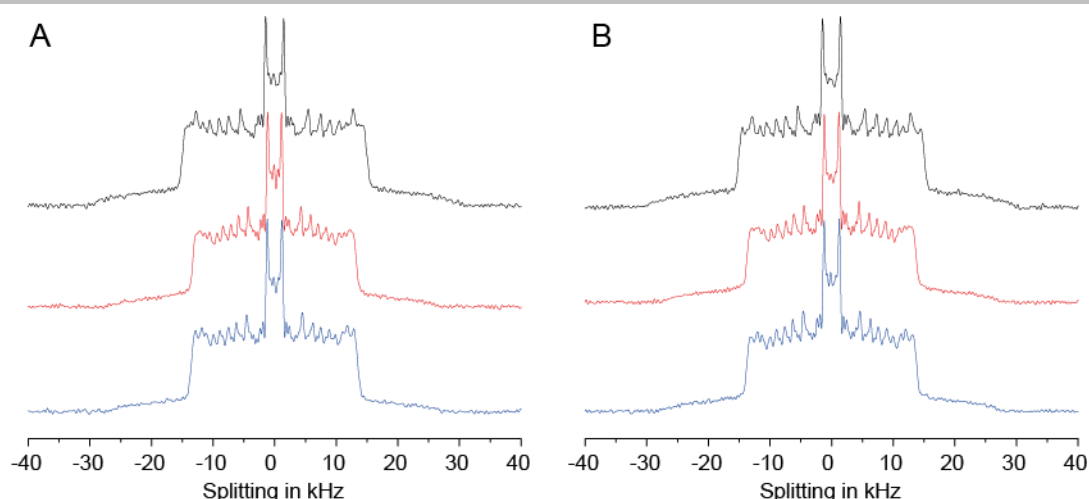


Figure S8. Resolved powder pattern for static ^2H NMR in G(-) IM. (A) POPG- d_{31} and (B) POPE- d_{31} in the pure G(-) IM lipid mixture (black lines). With WLBU2 (red lines) and D8 (blue lines) in the G(-) IM lipid mixture. Individual data are offset for ease of viewing.

The signals from POPG- d_{31} and POPE- d_{31} in the G(-) model in Fig. S8A,B are almost identical. This result fits well with expectations because the acyl chain is the only part of the lipid that is perdeuterated and no phase separation is expected. When the peptide is added the quadrupolar splitting is reduced. The effect is due to the larger averaged angle of the CD-bond vector plane with respect to the lipid principal axis. This directly translates to lower order parameters as shown in Fig S9.

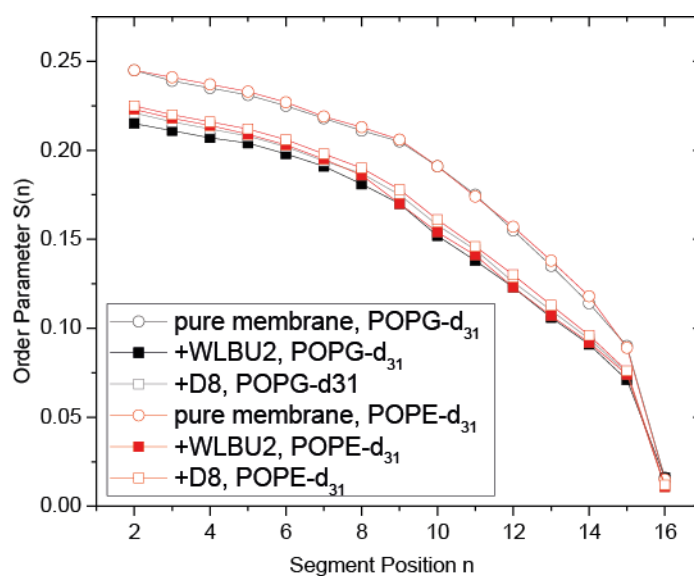


Figure S9. Calculated order parameter $S(n)$ from the static ^2H NMR-spectra of G(-) IM model with added peptides.

Table S16. Calculated chain extent of the deuterated palmitic chain from ^2H NMR for G(-) IM.

Chain extent (L_c^*) in Å for the palmitic chain in the deuterated lipid species		
	POPG- d_{31}	POPE- d_{31}
Pure membrane	12.3	12.4
+WLBU2	11.5	11.6
+D8	11.6	11.6

Table S16 shows a small bilayer thinning (~ 1.6 Å) which is in good agreement with the thinning observed by XDS (Fig. 2A in the main text). These results, combined with the ^{31}P NMR results shown in Fig. S7 and Table S15, suggest that the headgroups are pushed apart by both peptides upon binding, increasing the disorder in the lipid chains, thus thinning the bilayer. Hence, the increased ^{31}P CSA may reflect the reduced amplitude of motion for the lipid headgroups due to insertion of tryptophan side chains into the membrane-buffer interface.

SUPPORTING INFORMATION

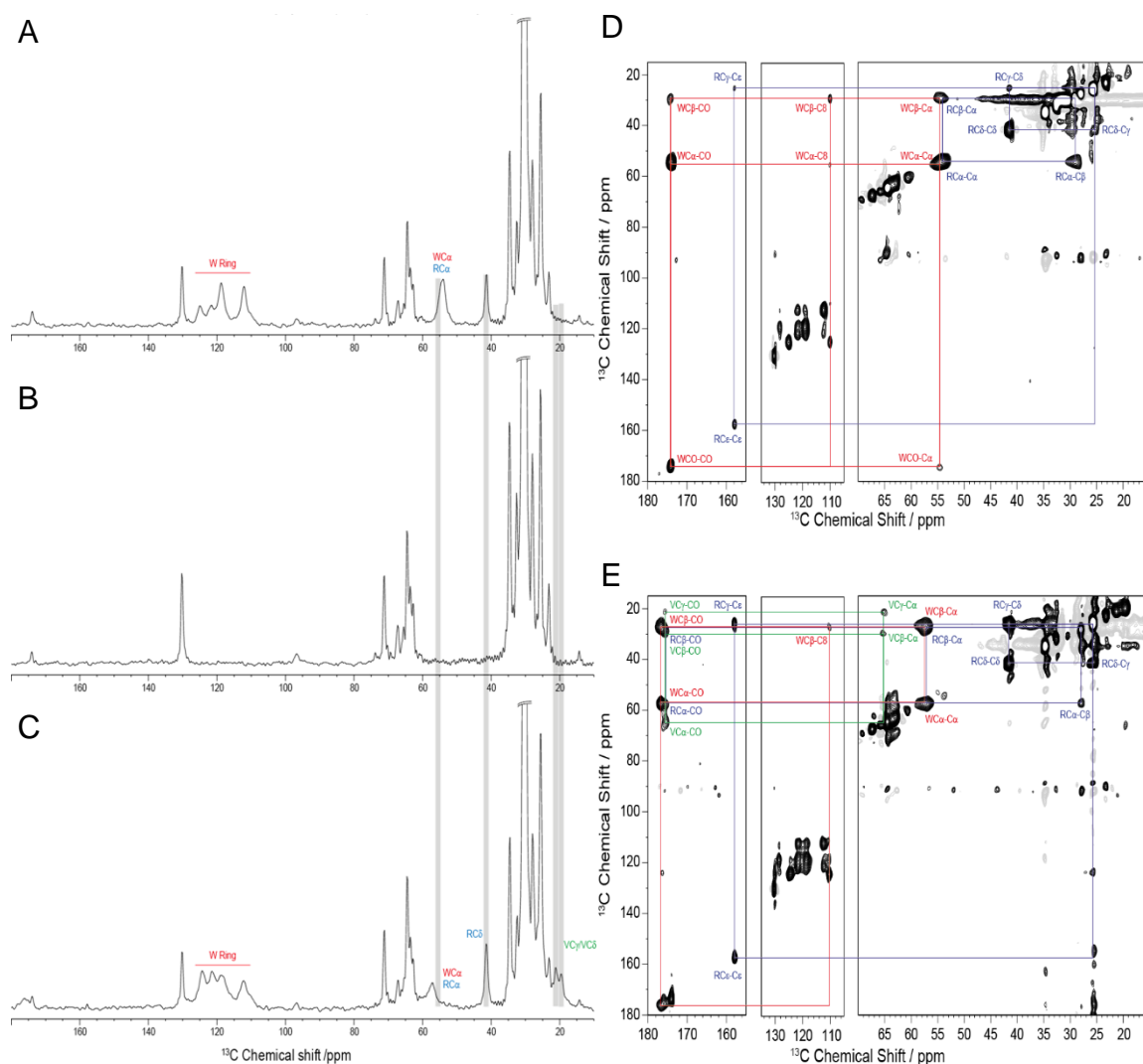


Figure S10. ^{13}C -MAS spectra for (B) G(-) IM control, (A) w/D8 and (C) w/WLBU2. Peaks are labeled in blue (R_5), red (W_{10}) and green (V_{15}). 2D ^{13}C - ^{13}C NMR spectra at 5kHz with all important shifts of labeled amino acids assigned. (D) D8 in G(-) IM, (E) WLBU2 in G(-) IM.

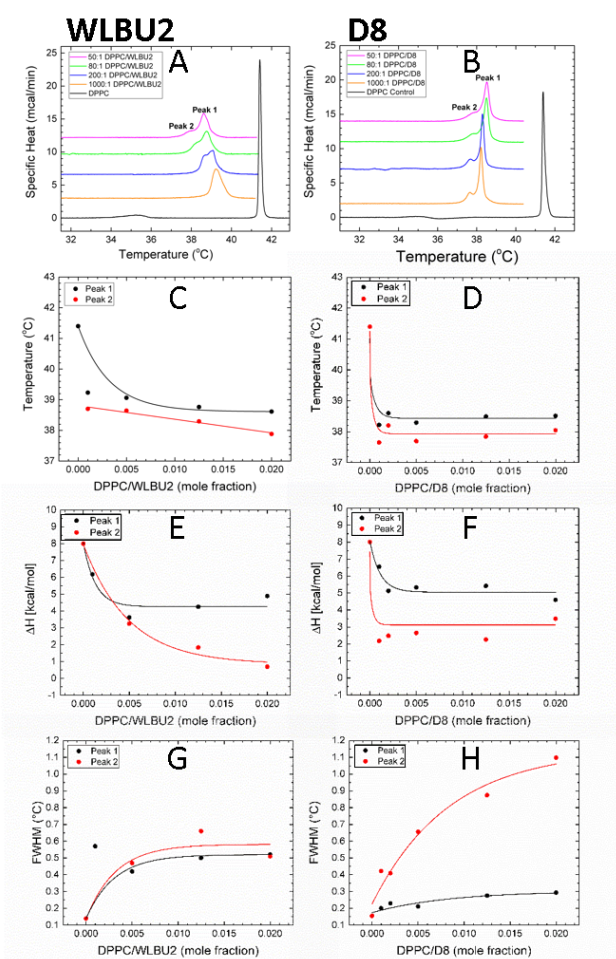
To elucidate the secondary structure of the peptides, we performed either solution or solid state magic angle spinning NMR. In WLBU2 R_5 , W_{10} and V_{15} were ^{13}C -labeled, but in D8 only R_5 and W_{10} were ^{13}C -labeled since labeled valines are not available as the D-enantiomers. Heteronuclear single quantum coherence-total correlation spectroscopy (HSQC-TOCSY) was used to determine that the solution structure of both WLBU2 and D8 are largely random coil in 15 mM PBS. When peptides are embedded in membranes, a solid state NMR method, dipolar assisted rotational resonance (DARR), was used to determine that WLBU2 is largely helical, while D8 remains in the random coil configuration. Compared to the pure G(-) (Fig.S10B), additional peaks are observed in Fig.S10A (D8) and S10C (WLBU2). We recorded 2D ^{13}C - ^{13}C NMR spectra to assign all peaks (Fig. S10D,E). The observed ^{13}C chemical shifts for the labeled peptides are summarized in Table S17. The number in parentheses denotes the number of times the peak was observed in the spectrum. A summary graph of these results is shown in the main paper in Fig. 4N,O. The same results were obtained for both peptides in the Euk50 model membrane (data not shown).

Table S17. Observed ^{13}C chemical shifts for labeled peptides in G(-) IM. N/A stands for not applicable and N/O stands for not observed.

AA in Peptide	CO	C α	C β	C γ	C δ	C ϵ	C ζ
R_5	WLBU2	175.5 \pm 0.1 (2)	57.3 \pm 0.1(3)	27.8 \pm 0.1(3)	26.0 \pm 0.2(3)	41.6 \pm 0.1(4)	157.8 \pm 0.2(3)
	D8	N/O	54.2 \pm 0.1(4)	29.4 \pm 0.3(4)	25.2 \pm 0.1(4)	41.4 \pm 0.2(5)	157.8 \pm 0.1(3)
W_{10}	WLBU2	176.7 \pm 0.1(2)	57.4 \pm 0.1(4)	26.8 \pm 0.1(3)	N/A	N/A	N/A
	D8	174.2 \pm 0.2(3)	54.9 \pm 0.3(6)	29.1 \pm 0.3(3)	N/A	N/A	N/A
V_{15}	WLBU2	175.5 \pm 0.1(3)	65.1 \pm 0.4(3)	29.8 \pm 0.1(2)	21.2 \pm 0.1(2)	N/O	N/A
	D8	Not labeled					

SUPPORTING INFORMATION

Differential Scanning Calorimetry (DSC).



The DSC traces for DPPC with lipid:peptide molar ratios 1000:1 (orange), 200:1 (blue), 80:1 (green), 50:1 (magenta) are shown in Fig. S11A,B, melting temperatures (Fig. S11C,D), enthalpies (Fig. S11E,F) and peak widths (Fig. S11G,H) as a function of added peptide. Fig. S12 shows how the decomposition of the main phase transition peak of DPPC with WLBUE2 was carried out. Fig. S13 shows how the decomposition of the main phase transition peak of DPPC with D8 was carried out.

Figure S11. Differential Scanning Calorimetry. Specific heat as a function of temperature for DPPC with (A) WLBUE2 or (B) D8 at different molar ratios DPPC:peptide: control lipid (black) 1000:1 (orange), 200:1 (blue), 80:1 (green), 50:1 (magenta). Scans are offset for ease of viewing. Panels (C-H) Peak 1 (black trace), Peak 2 (red trace). (C,D) Peak temperature as a function of mole fraction. (E,F) Peak enthalpy as a function of mole fraction. (G,H) Full width at half maximal height of peaks as a function of mole fraction. Scan rate was 12.7 °C/h.

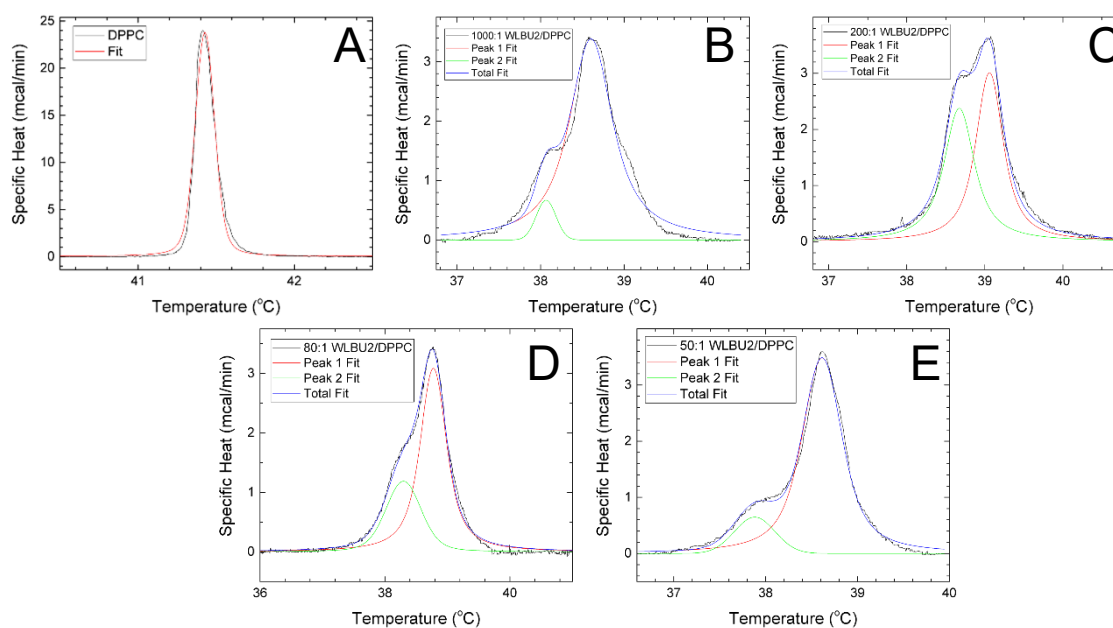


Figure S12. Decomposition of main melting transition of DPPC with WLBUE2 using a Voigt fitting, which is a combination of a Gaussian and a Lorentzian fitting. (A) Pure DPPC, DPPC/WLBUE2 molar ratios: (B) 1000:1, (C) 200:1, (D) 80:1, (E) 50:1.

SUPPORTING INFORMATION

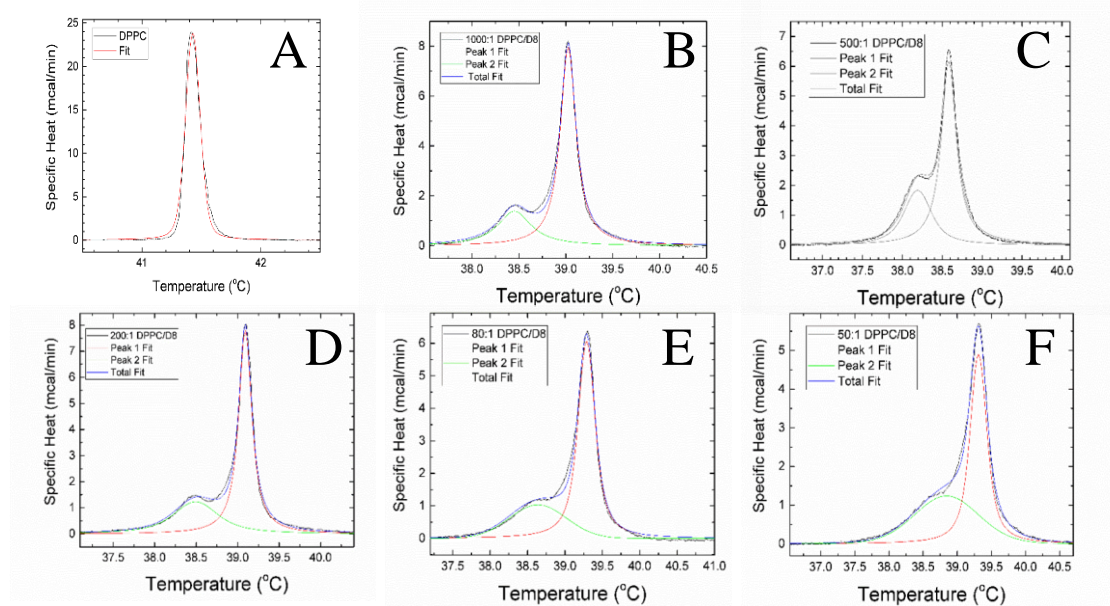


Figure S13. The main melting transition of DPPC with D8 was decomposed using a Voigt fitting. (A) Pure DPPC, DPPC/D8 molar ratios: (B) 1000:1, (C) 500:1, (D) 200:1, (E) 80:1, (F) 50:1.

MD simulation.

Fig. S14 shows the MD simulation results when WLBU2 was added to KDO2. In Fig. S14A, the form factor that results from the MD simulation is directly compared to that from the XDS experiment for pure KDO2. For this comparison we used the MD simulation with the doubly deprotonated phosphate groups, with a net negative charge of -6 for KDO2 and 432 sodium ions (6/lipid). As shown there is remarkable agreement between these two form factors, verifying that the force fields used in the simulation are correct. The sodium ions were not included in this comparison since the agreement is worse when they are included. The reason for this could be because the counterion used in the XDS experiment was the ammonium ion, not sodium, which has a lower electron density and so does not contribute to XDS form factors. Fig. S14B shows the electron density profile (EDP) that results by entering the simulation results into the SimtoExp computer program, with component groups as in the caption. As shown, there is a double headgroup peak, due to the electron density of the two octulosonic acid residues exterior to the phosphate groups. Fig. S14C shows a visualization of the KDO2 simulation, prepared using VMD. Colors are described in the caption. Fig. S14D shows the comparison of form factors for the case where WLBU2 was added to KDO2 (75:1 lipid:peptide molar ratio). In this case the singly deprotonated phosphate groups were used, giving a net negative charge of -4 to KDO2. Again, there is strikingly good agreement, showing that the protonation method did not affect these comparisons. In Fig. S14E, the EDP shows the location of WLBU2 in the outer headgroup region of KDO2, outside of the octulosonic acid residues. This is shown visually in Fig. S14F, where WLBU2 was initially constrained as an α -helix, since our CD results found it to be primarily helical in KDO2. When all constraints were removed, WLBU2 remained helical. D8 was not able to be simulated since the force fields for the D-amino acids mixed with L-amino acids have not been perfected.

SUPPORTING INFORMATION

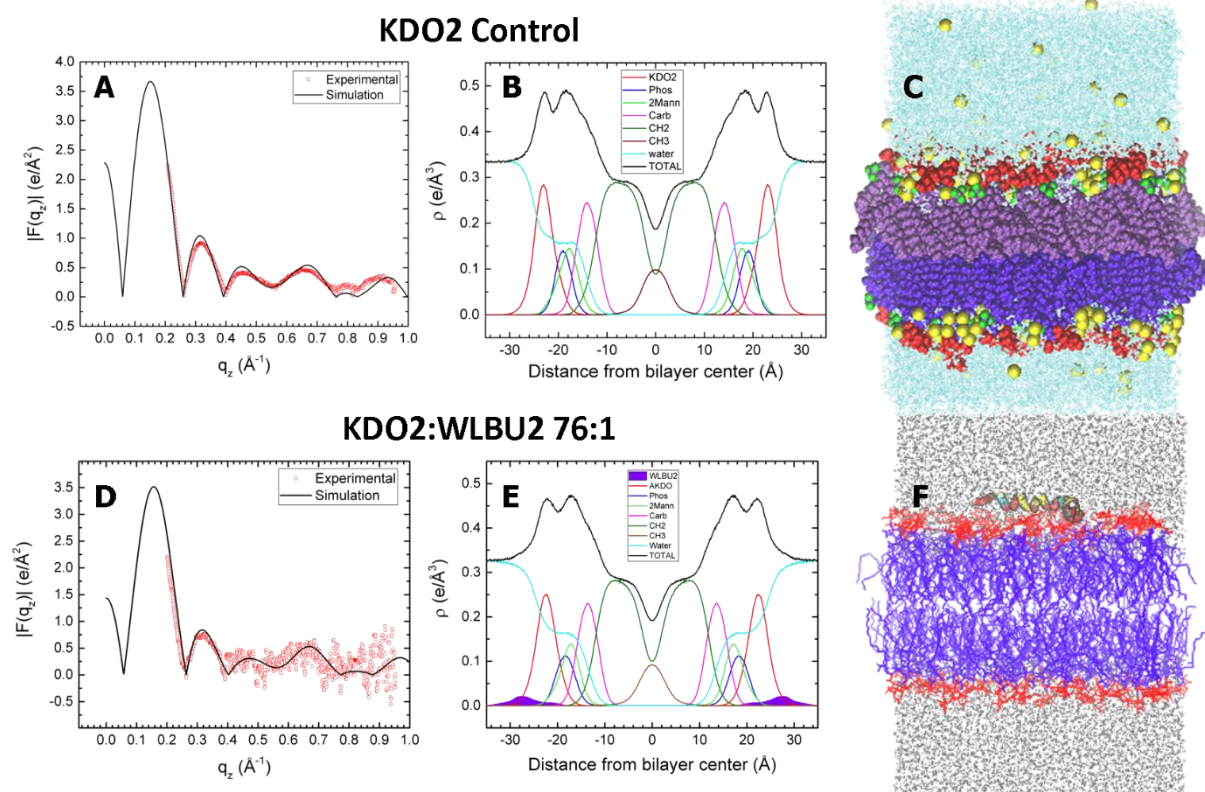


Figure S14. MD simulation results. (A) KDO2 control simulated form factors (black trace) and experimental (red open circles). (B) KDO2 control EDP. Colors: total, black; octulosonic acids, orange; phosphate groups, blue; mannoses, green; carbonyls, magenta; CH2 region, olive; CH3 trough, brown; WLB2, filled purple. (C) VMD visualization. Colors: lipid chains, lavender and purple; phosphate groups, green; octulosonic acids, red; sodium ions, yellow; water, cyan. (D) KDO2/WLB2 (75:1), colors as in (A). (E) KDO2/WLB2 (75:1) EDP, colors as in (B). (F) VMD visualization. Colors: lipid chains, purple; octulosonic acids, red; water, grey; WLB2, R, red, V, yellow, W, blue.

SI Acknowledgments

The authors thank Belita Opene (UMaryland-Baltimore) for purifying the PA01 LPS, Prof. Emeritus John F. Nagle, Megan Roche, Yasmene Elhady and Diamond Moody for help with the data collection at CHESS, and Dr. Arthur Woll for his help at the G1 CHESS beamline. This work is based upon research conducted at Carnegie Mellon University and at the Cornell High Energy Synchrotron Source (CHESS), which is supported by the National Science Foundation (NSF) under award No. DMR-1332208. Parts of this research were performed at the NIST Center for Nanoscale Science. Certain commercial materials, equipment, and instruments are identified in this work to describe the experimental procedure as completely as possible. In no case does such an identification imply a recommendation or endorsement by NIST, nor does it imply that the materials, equipment, or instrument identified are necessarily the best available for the purpose. The neutron work was supported by the Department of Commerce through its Measurement Science and Engineering Program (70NANB13H009), the National Institute of Standards and Technology (NIST) Center for Neutron Research Comprehensive Grant Program (70NANB17H299), and the NIST IMS Program "Precision Measurements for Integral Membrane Proteins". Additional support for this work was from National Institutes of Health (NIH) R01AI133351 (STN, YPD), NIH R01GM125917 (STN, BD), Carnegie Mellon SURF (AK, AS), CONICET, Programa de Becas Externas (FGD), National Science Foundation (NSF) OC1-1053575 (AP, JCG), NIH R01GM101647 (FH), German Research Foundation (DFG) HU 720/15-2 (DH).

SUPPORTING INFORMATION

References

- [1] S. A. Tristram-Nagle, *Methods Mol Biol* **2007**, *400*, 63-75.
- [2] N. Kučerka, Y. F. Liu, N. J. Chu, H. I. Petrache, S. T. Tristram-Nagle, J. F. Nagle, *Biophys J* **2005**, *88*, 2626-2637.
- [3] F. G. Dupuy, I. Pagano, K. Andenoro, M. F. Peralta, Y. Elhady, F. Heinrich, S. Tristram-Nagle, *Biophys J* **2018**, *114*, 919-928.
- [4] Y. Lyatskaya, Y. Liu, S. Tristram-Nagle, J. Katsaras, J. F. Nagle, *Phys Rev E Stat Nonlin Soft Matter Phys* **2001**, *63* (1 Pt 1), 011907.
- [5] Y. Liu, J. F. Nagle, **2004**, *Phys Rev E Stat Nonlin Soft Matter Phys*, *69* (4 Pt 1), 040901.
- [6] N. Kučerka, J. F. Nagle, J. N. Sachs, S. E. Feller, J. Pencer, A. Jackson, J. Katsaras, *Biophys J* **2008**, *95*, 2356-2367.
- [7] N. Kučerka, S. Tristram-Nagle, J. F. Nagle, *J Membrane Biol* **2005**, *208*, 193-202.
- [8] S. Tristram-Nagle, D. J. Kim, N. Akhuzada, N. Kucerka, J. C. Mathai, J. Katsaras, M. Zeidel, J. F. Nagle, *Chem Phys Lipids* **2010**, *163*, 630-637.
- [9] N. Kučerka, S. Tristram-Nagle, J. F. Nagle, *Biophys J* **2006**, *90*, L83-L85.
- [10] A. Kumagai, F. G. Dupuy, Z. Arsov, Y. Elhady, D. Moody, R. K. Ernst, B. Deslouches, R. C. Montelaro, Y. P. Di, S. Tristram-Nagle, *Soft Matter* **2019**, *15*, 1860-1868.
- [11] S. G. Wilkinson, *Microbial Lipids*, Vol. I, Academic Press, San Diego, CA, **1988**
- [12] J. De Gier, L. L. Van Deenen, *Biochim Biophys Acta* **1961**, *49*, 286-296.
- [13] J. Pan, D. P. Tieleman, J. F. Nagle, N. Kucerka, S. Tristram-Nagle, *Biochim Biophys Acta* **2009**, *1788*, 1387-1397.
- [14] R. T. Zhang, R. M. Suter, J. F. Nagle, *Phys Rev E* **1994**, *50*, 5047-5060.
- [15] M. Barros, F. Heinrich, S. A. K. Datta, A. Rein, I. Karageorgos, H. Nanda, M. Losche, *J Virol* **2016**, *90*, 4544-4555.
- [16] J.A. Dura, D. J. Pierce, C. F. Majkrzak, N. C. Maliszewskij, D. J. McGillivray, M. Losche, K. V. O'Donovan, M. Mihailescu, U. Perez-Salas, D. L. Worcester, S. H. White, *Rev Sci Instrum* **2006**, *77*, 74301-743011
- [17] F. Heinrich, M. Losche, *Biochim Biophys Acta Biomembr* **2014**, *1838*, 2341-2349.
- [18] B. J. Kirby, P. A. Kienzle, B. B. Maranville, N. F. Berk, J. Krycka, F. Heinrich, C. F. Majkrzak, *Curr Opin Colloid In* **2012**, *17*, 44-53.
- [19] Kern, W. *J Electrochem Soc* **1990**, *137*, 1887-1892.
- [20] R. Budvytyte, G. Valincius, G. Niaura, V. Voiciuk, M. Mickevicius, H. Chapman, H. Z. Goh, P. Shekhar, F. Heinrich, S. Shenoy, M. Losche, D. Vanderah, *Langmuir* **2013**, *29*, 8645-8656.
- [21] S. Brahmms, J. Brahmms, *J Mol Biol* **1980**, *138*, 149-178.
- [22] D. Huster, K. Arnold, K. Gawrisch, *Biochemistry* **1998**, *37*, 17299-17308.
- [23] J. Schiller, M. Muller, B. Fuchs, K. Arnold, D. Huster, *Curr Anal Chem* **2007**, *3*, 283-301.
- [24] W. Lee, M. Tonelli, J.L. Markley, *Bioinformatics* **2015**, *31*, 1325-1327.
- [25] B. Maggio, J. M. Sturtevant, R. K. Yu, *J Biol Chem* **1987**, *262*, 2652-2659.
- [26] C. Balusek, J. C. Gumbart, *Biophys J* **2016**, *111*, 1409-1417.
- [27] J. C. Phillips, R. Braun, W. Wang, J. Gumbart, E. Tajkhorshid, E. Villa, C. Chipot, R. D. Skeel, L. Kale, K. Schulten, *J Comput Chem* **2005**, *26*, 1781-1802.
- [28] J. B. Klauda, R. M. Venable, J. A. Freites, J. W. O'Connor, D. J. Tobias, C. Mondragon-Ramirez, I. Vorobyov, A. D. MacKerell, R. W. Pastor, *J Phys Chem B* **2010**, *114*, 7830-7843.
- [29] J. Huang, S. Rauscher, G. Nawrocki, T. Ran, M. Feig, B. L. de Groot, H. Grubmuller, A. D. MacKerell, *Nat Methods* **2017**, *14*, 71-73.
- [30] T. Darden, D. York, L. Pedersen, *J Chem Phys* **1993**, *98*, 10089-10092.
- [31] S. E. Feller, Y. H. Zhang, R. W. Pastor, B. R. Brooks, *J Chem Phys* **1995**, *103*, 4613-4621.
- [32] W. L. Jorgensen, J. Chandrasekhar, J. D. Madura, R. W. Impey, M. L. Klein, *J Chem Phys* **1983**, *79*, 926-935.
- [33] N. Kučerka, J. Katsaras, J. F. Nagle, *J Membrane Biol* **2010**, *235*, 43-50.
- [34] T. J. Pinheiro, A. Watts, *Biochemistry* **1994**, *33*, 24592467.
- [35] P. R. Cullis, B. de Kruffy, *Biochim Biophys Acta Biomembr* **1976**, *436*, 523-540.